A Comparative Investigation of Co²⁺ and Mn²⁺ Incorporation into Aluminophosphates by in Situ XAS and DFT Computation

Mei Dong,[†] Guofu Wang,[†] Zhangfeng Qin,[†] Jianguo Wang,*,[†] Tao Liu,[‡] Shuping Yuan,[†] and Haijun Jiao[†,§]

State Key Laboratory of Coal Conversion, Institute of Coal Chemistry, Chinese Academy of Sciences, Taiyuan, Shanxi 030001, P. R. China, Beijing Synchrotron Radiation Laboratory, Institute of High Energy, Chinese Academy of Sciences, Beijing, 100039, P. R. China, and Leibniz-Institut für Katalyse e.V. an der Universität Rostock, Albert-Einstein-Strasse 29a, 18059 Rostock, Germany

Received: September 29, 2006; In Final Form: December 11, 2006

The incorporation processes of Mn²⁺ and Co²⁺ into the framework of aluminophosphate molecular sieve AlPO₄-5, at the onset of crystallization, were investigated by in situ synchrotron X-ray absorption spectroscopy (XAS) and density functional theory (DFT) computation. The results indicated that the syntheses of MnAPO-5 and CoAPO-5 were different in the incorporation mechanism of metal ions. For the synthesis of CoAPO-5, Co²⁺ transferred from an octahedral into tetrahedral structure with crystal formation, while, for MnAPO-5, the Mn²⁺ transition to the tetrahedral structure was much more difficult and it occurred after the appearance of long-range ordered microporous structure. The DFT computations of model intermediates involved in the synthesis process suggested that much higher transformation energy of $[Mn(OP(OH)_3)_4]^{2+}$ than that of $[Co(OP(OH)_3)_4]^{2+}$ was responsible for the diversity of the incorporation behaviors.

Introduction

AlPO₄-5, an aluminophosphate molecular sieve with the topological structure of AFI, owns a unidirectional cylindrical channel of 12-membered rings with uniform cross sections of 0.73 nm along the *c*-axis. Such a channel opening, comparable to the molecule size of aromatics, suggests a potential application in catalysis. However, the neutral framework and lack of proper acidic/basic properties prohibit it from further applications. The isomorphous substitution of metal ions, such as Co²⁺, Mn²⁺, Fe³⁺, Cr³⁺, and Ti⁴⁺, into the framework of aluminophosphate molecular sieves (AlPO₄-*n*, where *n* denotes a particular structure type) may generate highly isolated active sites and unique regioselectivity and shape-selectivity and exhibit potential catalytic applications in the selective oxidation of alkanes and conversion of methanol to olefins.[1−3] Metal-substituted aluminophosphate-based microporous materials (MeAPOs) are generally hydrothermally synsesized from precursors containing metal ions and organic template molecules. To obtain MeAPOs with desired location of active sites and well-defined atomic environment, it is crucial to get insights into the transition process of metal ion from the precursor gel into the framework.[4,5]

Considerable efforts have been devoted to understanding the transformation of amorphous precursor to crystal with microporous structures in the hydrothermal process. Ex situ studies, by sampling the crystallization at regular intervals and subjecting the samples to various physical characterizations, have provided certain useful information. Arieli et al.[6] explored the process of Mn²⁺ incorporation into AlPO₄-5 and AlPO₄-11 by combined electron−nuclear double resonance (ENDOR) spectroscopy and DFT calculation and suggested that the aluminophosphate

network was formed prior to the detection of an X-ray diffraction (XRD) pattern and gradually transformed to the three-dimensional crystalline structures. Tan et al.[7] investigated the incorporation of Si into SAPO-34 by means of XRD, scan electron microscopy (SEM), X-ray fluorescence spectroscopy (XRF), infrared spectroscopy (IR), and nuclear magnetic resonance spectroscopy (NMR); they proposed that Si was incorporated via a direct participation mechanism in the early stage and then a substitution mechanism in the later stages. However, it is inevitable that lots of clues may be lost upon the quenching, washing, and drying for the ex situ study. More detailed and reliable information can be obtained by performing in situ measurements.

In situ XRD,[8−12] X-ray absorption spectroscopy (XAS),[13−15] small-angle/wide-angle X-ray scattering (SAXS/WAXS),[15−17] neutron diffraction,[18,19] ultraviolet/visible spectrometry (UV/vis),[20] NMR,[21] Raman spectroscopy,[15,22] and FT-IR spectroscopy[23] have been proved to be effective in tracking the hydrothermal crystallization of molecular sieves. Various information of nucleation, kinetics of growth, nature of molecular species, and identification of intermediate phases has been obtained depending on the special in situ techniques used.[24] Christensen et al.[8,9,11] investigated the crystallization of microporous aluminophosphates and Mg²⁺-, Mn²⁺-, Co²⁺-, and Zn²⁺-substituted aluminophosphates by in situ synchrotron XRD. The kinetic analysis based on the isothermal XRD suggested that the nature of the transition metal cations has significant influence on the crystallization rate and mechanism. Furthermore, the amounts of metal ions in the precursor gel also decide the formation of crystal with AFI, AEI, and CHA structures in a competitive way and affect the properties of the synthesized molecular sieves.[25,26] In situ XRD can identify the species with long-range ordered structure but give little information on the amorphous materials related to the hydrolysis, aggregation, oligomerization, and nucleation in a hydrothermal process.[27,28] On the other hand, SAXS can provide information

* Author to whom correspondence should be addressed. E-mail: iccjgw@sxicc.ac.cn. Tel: +86-351-4046092. Fax: +86-351-4041153.
† Institute of Coal Chemistry, Chinese Academy of Sciences.
‡ Institute of High Energy, Chinese Academy of Sciences.
§ Leibniz-Institut für Katalyse e.V. an der Universität Rostock.

Figure 1. Synthesis cell for in situ XAS (left) and that with Be windows and heating component mounted (right).

about the dimension, shape, and number of small species that are sensitive to the structure of nuclei formed during the induction period. It has been observed that the nuclei particles in the precursor gel have broad size distribution from several to decades nanometers dimension before the onset of crystallization.[15−17] Other in situ techniques, such as Raman and FT-IR can also provide information related to the intermediate species formed during the crystallization. XAS, both X-ray absorption near-edge structure (XANES) and extended X-ray absorption fine structure (EXAFS), hold promise for studying the synthesis of molecular sieves in situ, which is possible to detect a specific chemical constitute in the synthesis system selectively, even as it is highly diluted, and to probe its site environment in terms of bond distance and coordination number. XAS is easy to perform with the aid of synchrotron radiation sources, which provide a broad-band, tunable source of radiation with uniform intensity in the X-ray region. When compared to conventionally generated X-rays, the high brightness of synchrotron radiation makes it possible to collect high-resolution data in a short time. The in situ synchrotron XAS during CoAPO-5 crystallization reveals that the incorporation of Co^{2+} is prior to the crystal formation.[13,15]

Although a large number of studies referred to the synthesis of MeAPOs, only a small part of them concerned the detailed process of metal incorporation into the aluminophosphate framework during the hydrothermal synthesis. There is little knowledge of the transient of active ion from the precursor gel to the templated solid microporous materials; this makes it difficult to synthesize these microporous materials designedly with desired location of active sites and well-defined atomic environment. It has been suggested that the heteroatom species have vital influence not only on the crystallization rate and mechanism but also on the crystal structure formed. For example, the apparent activation energies for the hydrothermal nucleation of MnAPO-5 (AFI) and ZnAPO-47 (CHA) have been determined as 161 and 113 kJ/mol, respectively, by the kinetic analysis of the isothermal in situ synchrotron XRD data in crystallization.[11] However, the intrinsical influence of metal ions on the crystallization is still unclear.

In this work, in situ synchrotron XAS was applied to investigate the hydrothermal crystallization process of Co^{2+}- and Mn^{2+}-substituted $AlPO_4$-5. The detailed transformation processes of these two metal ions from the amorphous precursor gel to the crystal were described. To get insight into the intrinsical difference of the metal ions, DFT computations were performed on the Co^{2+} and Mn^{2+} intermediates formed in the synthesis process.

Experimental Section

The precursor gels of aluminophosphate-containing metal ions (Co^{2+} or Mn^{2+}) were synthesized according to the verified method.[29,30] Chemicals involved in the synthesis are H_3PO_4 (Tianjin Tianda Chemical Co., 85%), pseudoboehmite Al_2O_3 (Shandong aluminum Co., 77%), triethylamine (TriEA, Tianjin Fuchen Chemical Co., >99%), $Mn(CH_3COO)_2 \cdot 4H_2O$ (Beijing Chemical Co., >99%), and $Co(NO_3)_2 \cdot 6H_2O$ (Sinopharm Chemical Reagent Co., >99%). In a typical synthesis process, TriEA as the template was added into the mixture of orthophosphoric acid, pseudoboehmite alumina, and $Co(NO_3)_2 \cdot 6H_2O$ or $Mn(CH_3COO)_2 \cdot 4H_2O$ under intensive stirring. This mixture was stirred continuously and aged for a further 60 min, and the precursor gels with the molar ratio of $MeO:Al_2O_3:P_2O_5:TriEA:H_2O$ being 0.12:0.44:0.6:0.84:22, where Me = Co or Mn, were obtained.

A special synthesis cell as shown in Figure 1 was designed to meet the demands of both the hydrothermal process and the in situ XAS measurement. Beryllium windows with a thickness of 0.5 mm were used in both sides of the synthesis cell, and the length of X-ray light route in the cell was set at 3 mm. A heating component was mounted around the synthesis cell, and a thermocouple was inserted into the cell. The temperature of synthesis system was monitored and programmed with a temperature controller.

XAS measurements were carried out at the 1W1B beam line of Beijing Synchrotron Radiation Facility (BSRF). The precursor gel was sealed in the in situ cell and then subjected to synchrotron X-ray. It was then heated from ambient temperature to 200 °C at a heating rate of 5 °C/min. During this process, the environmental change of metal ions during the crystallization of MeAPOs was monitored by quick EXAFS (QEXAFS) technique in the transmission mode with an acquisition time of 80−90 s.[31,32]

The X-ray absorption spectra obtained were analyzed with the program WinXAS.[33,34] The background correction and normalization were carried out by fitting a linear polynomial to the preedge region and square polynomial to the postedge region of the absorption spectrum. The E_0 value was determined by the maximum in the first derivative in the edge region. Fourier transformations were performed on k^3-weighted EXAFS oscillations in the range $3−11$ Å$^{−1}$, employing Gaussian windows. For the fitting of the first coordination shell, the phase shifts and backscattering magnitudes were derived from a theoretical calculation from a standard using the FEFF6 code.[35] The crystallographic data on CoO and MnO served as a basis for the atomic configurations. The uncertainties of the obtained Debye−Waller factor, Me−O (Me = Co, Mn) coordination

Co²⁺ and Mn²⁺ Incorporation into Aluminophosphates

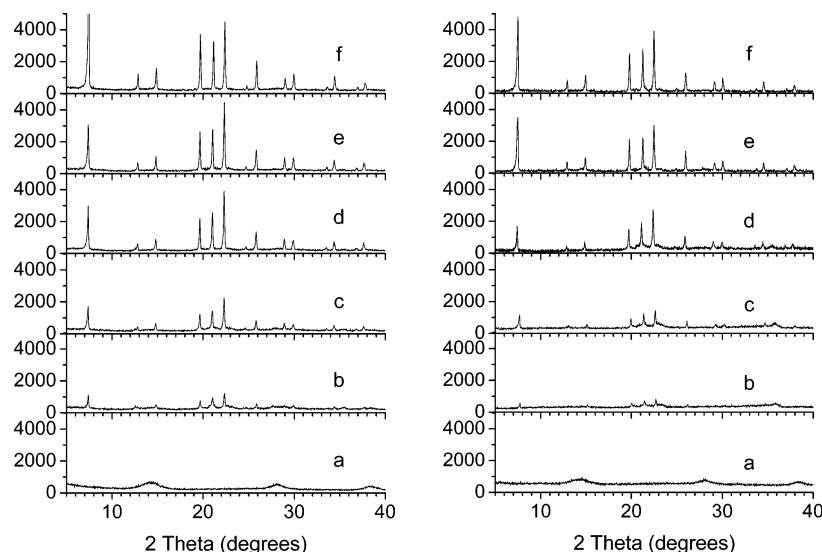*J. Phys. Chem. A, Vol. 111, No. 8, 2007* **1517**

Figure 2. XRD patterns of MnAPO-5 (left) and CoAPO-5 (right) with the crystallization temperature: (a) 140 °C; (b) 150 °C; (c) 170 °C; (d) 190 °C; (e) 200 °C; (f) 200 °C kept for 60 min.
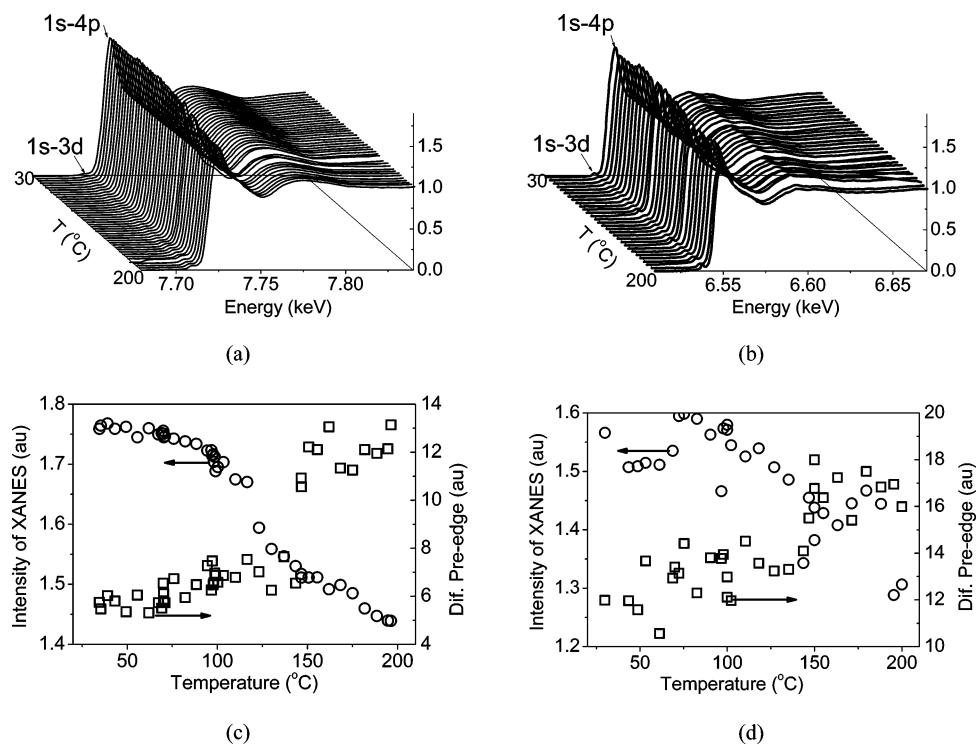

Figure 3. Three-dimensional stack plots of the background-subtracted and normalized XANES spectra at the Co K edge and Mn K edge recorded in situ during crystallization of (a) CoAPO-5 and (b) MnAPO-5 (b), respectively, starting from the precursor gel. Also shown are the integrated intensity of the white line feature (O) and differential preedge feature (□) as a function of crystallization temperature for (c) CoAPO-5 and (d) MnAPO-5.

number, and bond distance are estimated within $\pm 3 \times 10^{-5}$ Å², ± 0.01, and ± 0.002 Å, respectively.

In addition, to monitor the formation of crystal with long-range ordered structure, the content in the synthesis cell was sampled at various periods and the samples were subjected to the ex situ XRD characterization. The same synthesis cell as described above, acting as an autoclave, was adopted considering the consistency of the in situ and ex situ measurements. For the sampling, the cell was quenched in a water bath right after the content inside reached a given temperature (140, 150, 170, 190, and 200 °C); then the powder samples were recovered by filtrating, washing, and drying at 120 °C overnight. XRD was preformed on a Rigaku D/max-2500 X-ray diffraction spectrometer with Cu Kα radiation (0.154 18 nm, 40 kV, and 100

mA) in the range of 2θ between 5 and 40°. Because of the low crystallinity of the samples and bad resolution of the patterns involved, the analysis of the cell parameters of as-synthesized products is neglected in the work.

Computational Details

All calculations were done with the Dmol3 program as implemented in the Material Studio 2.2 package of Accelrys Inc.[36−39] The doubled numerical basis set with polarization functions (DNP) and generalized gradient approximation (GGA) functional by Becke exchange plus Lee−Yang−Parr correlation (BLYP)[40,41] was used. The tolerances of energies, gradient, and displacement convergence were 1×10^{-5} au, 2×10^{-3} au/Å,
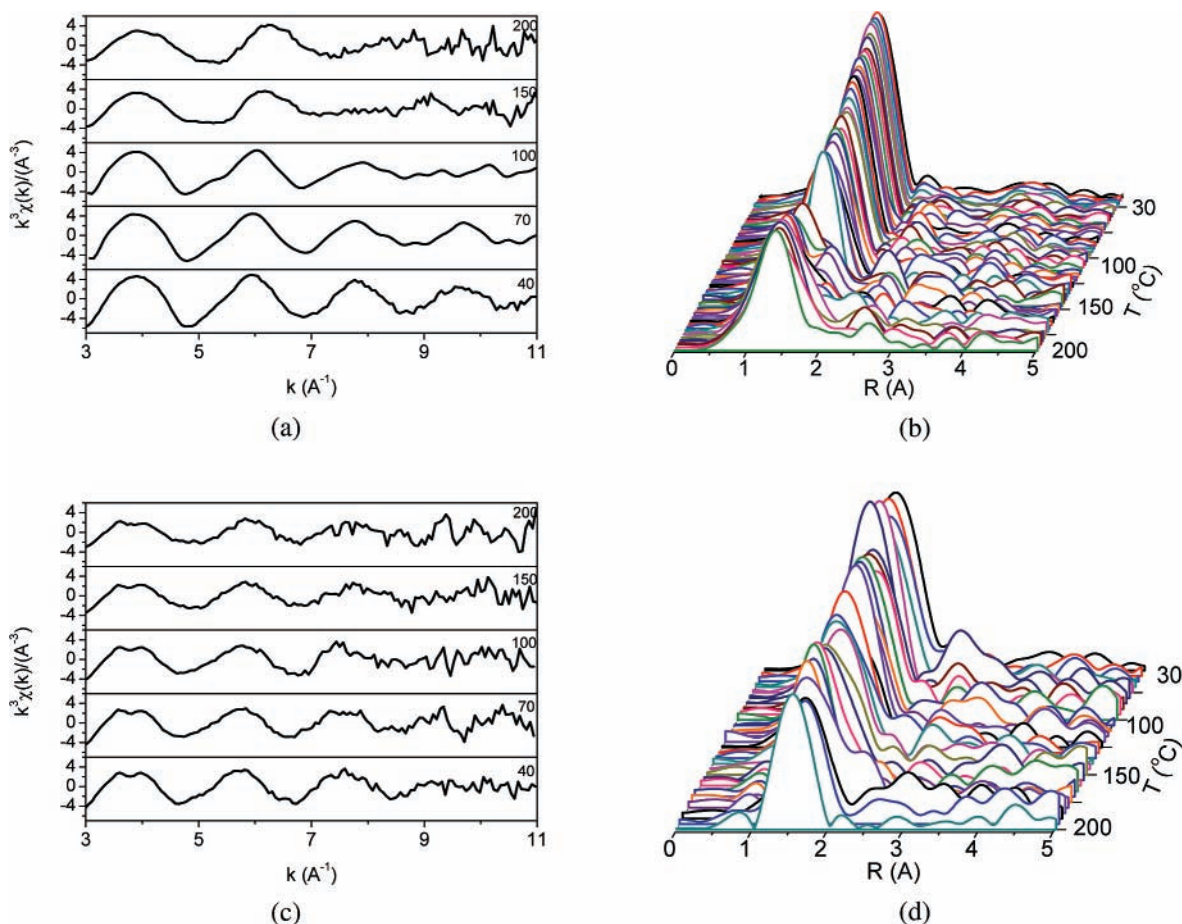
Figure 4. (a, c) k^3-weighted XAFS oscillations and (b, d) corresponding three-dimensional stack plots of the Fourier transforms of EXAFS data (k^3-weighted over k range from 3 to 11 Å^{-1}) recorded in situ during the crystallization of (a, b) CoAPO-5 and (c, d) MnAPO-5 obtained at different crystallization temperature; for XAFS oscillations, from bottom to top: 40 °C; 70 °C; 100 °C; 150 °C; 200 °C.

and 5×10^{-3} Å, respectively. The real space cutoff of atomic orbitals was set at 4.5 Å.

Results and Discussion

Experimental Results. XRD patterns of MnAPO-5 and CoAPO-5 samples withdrawn at various crystallization stages are shown in Figure 2. The crystalline aluminophosphates have the structure of AFI, characterized by the diffraction peaks at 2θ of 7.4, 19.6, 21.0, and 22.3°. It indicated that the samples obtained at 140 °C are amorphous, while the diffraction peaks appeared in the samples obtained at a crystallization temperature above 150 °C, for both MnAPO-5 and CoAPO-5. This was consistent with that from the in situ XRD studies, which demonstrated that the crystallization of aluminophosphate containing Co^{2+} and Mn^{2+} starts at the elevated temperature of 130−150 °C.[10,11] On the other hand, MnAPO-5 and CoAPO-5 exhibit little difference in the crystallinity and starting temperature for crystallization, as revealed by the XRD patterns.

The background-subtracted and normalized XANES at the Co and Mn K edge recorded in situ during the crystallization of CoAPO-5 and MnAPO-5, as well as the simultaneous variation of the absorption intensity and the differential preedge feature, as a function of the crystallization temperature are presented in Figure 3. The white line, i.e., electron transition of 1s to 4p, is sensitive to the local structure of metal ions. With the increase of temperature, the intensity of the white line decreases monotonously, while the peak width broadens considerably. This observation could be explained by the change of coordination environment (the local coordination environment

of Me^{2+} becomes more covalent with the crystallization) rather than by the change of ligand number and oxidation state of Me^{2+}.[15] When absorbing atoms exist in the environment with strong electrovalent bond, the dense electron cloud around Me^{2+} results in high potential barrier for electron capturing, which leads to a sharp absorption peak. However, the diluted electron cloud in the case of covalent environment brings on the electron capturing in wider range and a broader absorption peak. On the other hand, it is notable that the decrease in intensity for MnAPO-5 with increasing temperature is much less than that for CoAPO-5, indicating the difference in the coordination number changes.

The preedge feature at 7.708 and 6.538 keV for CoAPO-5 and MnAPO-5, respectively, originated from a 1s to 3d transition, is forbidden in centrosymmetric structures but is allowed in noncentrosymmetric ones such as tetrahedral or deformed octahedral structures. The Co preedge feature increases by about 3-fold upon crystallization, indicating Co^{2+} transformation from 6-fold to 4-fold coordination. However, the change in the Mn preedge is much less, suggesting a quadruple transition in the pseudooctahedral intermediates $[\text{Mn}(\text{H}_2\text{O})_x(\text{OP}(\text{OH})_3)_{6-x}]^{2+}$ from the reaction of Mn(H$_2$O)$_6^{2+}$ with H$_3$PO$_4$ or H$_2$PO$_4^-$.[15]

Figure 4 shows the k^3-weighted XAFS oscillations and corresponding three-dimensional stack plots of the Fourier transforms of the EXAFS spectra (k^3 weighted over k range from 3 to 11 Å^{-1}) during the crystallization of AlPO$_4$-5 containing Co^{2+} and Mn^{2+}. An intense peak, corresponding to the first coordination shell of oxygen, reduces monotonously with the crystallization from room temperature to 200 °C.
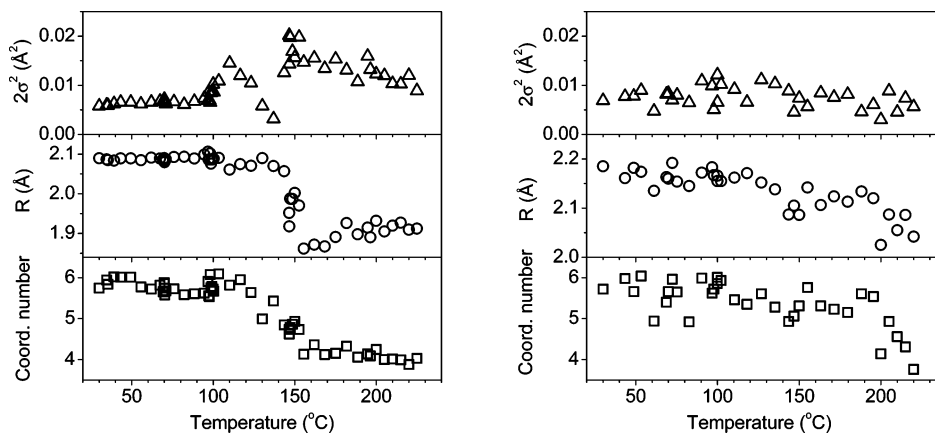
Co²⁺ and Mn²⁺ Incorporation into Aluminophosphates

J. Phys. Chem. A, Vol. 111, No. 8, 2007 **1519**

Figure 5. Evolution of Debye−Waller term $2\sigma^2$ ($\triangle$), coordination distance R ($\bigcirc$), and coordination number N ($\square$) of metal to oxygen coordination shell in the crystallization of CoAPO-5 (left) and MnAPO-5 (right) with temperature.

TABLE 1: Calculated Coordination Number and Me−O Distance in the Intermediates during the Synthesis of MeAPO-5 (Me = Co, Mn)

| compd | series | CN[a] | Me−O coord dist (Å) | | av value | ref[b] |
			Me−O(H)	Me−O(P)		
CoAPO-5	1	6(6,0)	2.15(4), 2.14(2)		2.15	2.11
	2	6(5,1)	2.17(2), 2.16, 2.15, 2.14	2.060	2.14	
	3	6(4,2)	2.14, 2.15, 2.16, 2.19	2.11, 2.09	2.14	
	4	6(3,3)	2.18(2), 2.17	2.16, 2.10, 2.06	2.14	
	5	6(2,4)	2.20, 2.16	2.15, 2.07, 2.18, 2.11	2.14	
	6	5(1,4)	2.20	2.07, 2.03, 2.07, 2.04	2.08	2.03
	7	4(0,4)		2.01, 1.97, 1.97, 2.00	1.99	1.94
MnAPO-5	1	6(6,0)	2.23(6)		2.23	2.19
	2	6(5,1)	2.24(3), 2.26, 2.27	2.10	2.22	
	3	6(4,2)	2.24, 2.25(2), 2.27	2.16(2)	2.22	
	4	6(3,3)	2.30, 2.28, 2.26	2.20, 2.16, 2.11	2.22	
	5	6(2,4)	2.31, 2.28	2.20, 2.13, 2.22, 2.18	2.22	
	6	5(1,4)	2.19	2.14(2), 2.06, 2.18	2.14	2.11
	7	4(0,4)		2.03(2), 2.08, 2.09	2.06	2.02

[a] Coordination number in $c(x,y)$, where x is the coordinated-oxygen number in the H_2O ligand, y is the coordinated-oxygen number in the H_3PO_4 ligand, and c is the overall coordinated-oxygen number. [b] Based on Shannon crystal radii and oxide radius of 1.22 Å.[44,45]

Figure 5 depicts the evolution of Debye−Waller term $2\sigma^2$, coordination distance, and coordination number of Me−O coordination shell with the crystallization of CoAPO-5 and MnAPO-5. For the crystallization of CoAPO-5, results similar to those by Grandjean et al.[15] are obtained. It reveals that the transition of Co²⁺ into the tetrahedral framework is via three stages: (i) a tiny but gradual decrease in the Co−O length from 2.09 Å to 2.07 Å with a Co²⁺ coordination number of 6 (up to 120 °C); (ii) a sharp decrease in the Co−O length to 1.92 Å, at the same time the Co²⁺ coordination number decreasing to 4 (120−150 °C); (iii) the Co−O length maintained at ca. 1.90−1.92 Å with a Co²⁺ coordination number of 4 (150−200 °C). On the other hand, the Debye−Waller factors associated with the Co−O shell increase with crystallization temperature and reach the highest value at 150 °C. The relatively high Debye−Waller factors for CoAPO-5 suggest that the coordination geometries of Co²⁺ are largely distorted, owing to the incorporation of Co²⁺ from the disordered reactant mixture into rigid microporous aluminophosphate.

However, the evolution of Mn−O exhibited obvious differences from that of Co−O in AlPO₄-5. As shown in Figure 5, the Mn−O length reduces from 2.18 Å in the precursor gel (corresponding to octahedral coordination) to 2.16 Å up to 100 °C and then to 2.08 Å at 200 °C, while the coordination number of Mn²⁺ changes from 6 to 5. The coordination distance and coordination number decrease further to 2.04 Å and 4, respectively, after crystallization for 30 min at 200 °C. It is obvious that the transformation of Mn²⁺ from 6-fold to 4-fold coordina-

tion is more difficult than that of Co²⁺. This is consistent with the order of apparent activation energies for the crystallization of MnAPO-5 (94 kJ/mol) and CoAPO-5 (61 kJ/mol) as determined by in situ XRD.[42]

DFT Computations. Metal ions, introduced into the reactant mixture with a pH value of 2−3, are in the hydrated form of $[Me(H_2O)_6]^{2+}$, where Me = Co²⁺ or Mn²⁺. Water ligands are gradually replaced by H_3PO_4 or $H_2PO_4^-$ to form the intermediates in 6-, 5-, and 4-fold coordination. Thus, a simple transformation model of metal ions from octahedral to tetrahedral structure, through the replacement of water in $[Me(H_2O)_6]^{2+}$ by H_3PO_4, was proposed.[6,20] As shown in Figure 6, the structures of the model intermediates start with the optimized $[Me(H_2O)_6]^{2+}$ (Me = Co, Mn, Figure 6-1). The structures of intermediates $[Me(H_2O)_{6-x}(OP(OH)_3)_x]^{2+}$ ($x = 1-4$) (Figure 6-2 to 6-5) are constructed by replacing H_2O ligands in $[Me(H_2O)_6]^{2+}$ gradually with $[OP(OH)_3]$ group. The structure of intermediates $[Me(H_2O)_x(OP(OH)_3)_4]^{2+}$ ($x = 0-1$) (Figure 6-6 to 6-7) comes from cutting off one or two H_2O molecules in the optimized $[Me(H_2O)_2(OP(OH)_3)_4]^{2+}$. It should be noted that phosphorus may exist as the oligomers of aluminophosphate in the actual synthesis process,[27] while large clusters with long aluminophosphate chains are unpractical for the DFT optimization. Therefore, the hydroxyl instead was used for phosphorus saturation in the present computation.[43]

The calculated Me−O coordination distances in the optimized intermediates and those based on the Shannon's crystal radii
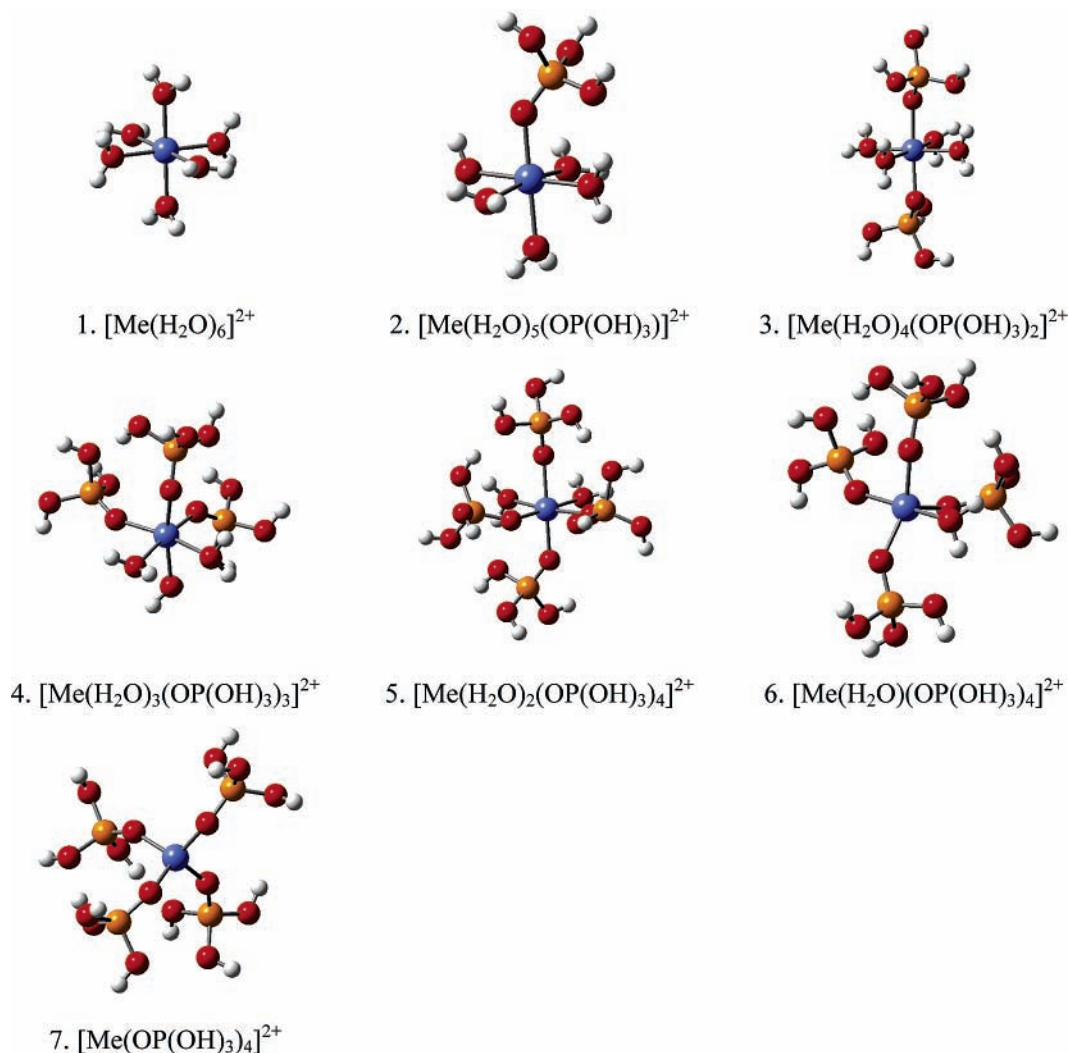
Figure 6. Optimized structure of the cluster model of intermediates in the synthesis of MeAPO-5 (orange, P atom; blue, Co or Mn, red, O; gray, H).
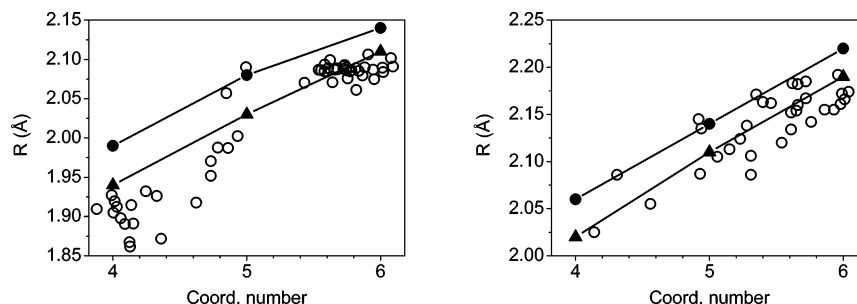

Figure 7. Co−O (left) and Mn−O (right) coordination distances as a function of the coordination number obtained from the in situ EXAFS (○), theoretical computation (●), and Shannon's crystal radii (▲).

(oxide radius of 1.22 Å)[44,45] are listed in Table 1. A comparison of the Co−O and Mn−O coordination distances as a function of the coordination number obtained from the in situ EXAFS, theoretical computation, and Shannon's crystal radii are illustrated in Figure 7. In the theoretical optimized intermediates, the Co−O and Mn−O lengths in the octahedral $[Me(H_2O)_6]^{2+}$ are 2.15 and 2.23 Å, respectively; with one water molecule replaced by H_3PO_4, they decrease slightly to 2.14 Å (Co−O) and 2.22 Å (Mn−O), respectively, and then keep constant for further substitution in the intermediates with 6-fold coordination. Exclusion of H_2O from the intermediates, corresponding to the change in the coordination number of Co^{2+} and Mn^{2+} from 6

to 5 and 4, results in the shrinking of Me−O distance. This trend agrees well with the changes in Me−O length obtained from the experimental results in this work and the calculated ones from the crystal radii,[44] although the absolute values may be some overestimated (Figure 7). Furthermore, Mn−O distance is longer than Co−O distance, also suggesting that the incorporation of Mn^{2+} into the Al−O−P network is much more difficult than that of Co^{2+}.

The total energies of optimized intermediates are listed in Table 2. It indicates that the exchange reaction of H_3PO_4 with water in the hydrated metal ions results in a decrease in the total energy.

Co^{2+} and Mn^{2+} Incorporation into Aluminophosphates

J. Phys. Chem. A, Vol. 111, No. 8, 2007 **1521**

TABLE 2: Computed Energies for Intermediates [Me(H$_2$O)$_x$(OP(OH)$_3$)$_y$]$^{2+}$ [a]

	tot energy (au)	
structures	Me = Mn^{2+}	Me = Co^{2+}
[Me(H$_2$O)$_6$]$^{2+}$	−580.122 58	−625.141 23
[Me(H$_2$O)$_5$(OP(OH)$_3$)$_1$]$^{2+}$	−1148.004 84	−1193.024 78
[Me(H$_2$O)$_4$(OP(OH)$_3$)$_2$]$^{2+}$	−1715.882 91	−1760.904 32
[Me(H$_2$O)$_3$(OP(OH)$_3$)$_3$]$^{2+}$	−2283.754 44	−2328.772 90
[Me(H$_2$O)$_2$(OP(OH)$_3$)$_4$]$^{2+}$	−2851.624 66	−2896.641 75
[Me(H$_2$O)$_1$(OP(OH)$_3$)$_4$]$^{2+}$	−2775.156 33	−2820.180 97
[Me(OP(OH)$_3$)$_4$]$^{2+}$	−2698.682 38	−2743.730 16
H$_2$O		−76.447 56
H$_3$PO$_4$		−644.310 83

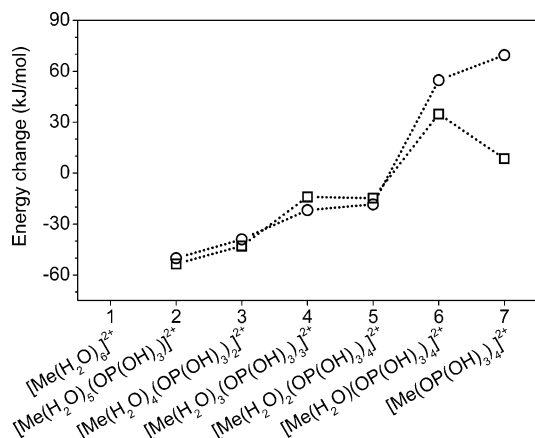[a] For [Me(H$_2$O)$_x$(OP(OH)$_3$)$_y$]$^{2+}$, Me = Co or Mn; $x + y$ = 6, 5, or 4; $x \leq 6$, $y \leq 4$.

Figure 8. Computed Co−O and Mn−O distances in different intermediates and stepwise reaction energies for the formation of intermediates [Me(H$_2$O)$_x$(OP(OH)$_3$)$_y$]$^{2+}$ ((□, Me = Co; ○, Me = Mn).

The energy changes (ΔE) for the stepwise transformation of the intermediates described in Figure 8 are calculated by

$$\Delta E_2 = (E_2 + E_{H_2O}) - (E_{H_3PO_4} + E_1) \qquad (1)$$

$$\Delta E_3 = (E_3 + E_{H_2O}) - (E_{H_3PO_4} + E_2) \qquad (2)$$

$$\Delta E_4 = (E_4 + E_{H_2O}) - (E_{H_3PO_4} + E_3) \qquad (3)$$

$$\Delta E_5 = (E_5 + E_{H_2O}) - (E_{H_3PO_4} + E_4) \qquad (4)$$

$$\Delta E_6 = E_6 + E_{H_2O} - E_5 \qquad (5)$$

$$\Delta E_7 = E_7 + E_{H_2O} - E_6 \qquad (6)$$

where E_1 denotes the energy of cluster [Me(H$_2$O)$_6$]$^{2+}$, E_2−E_5 denote the energies of clusters [Me(H$_2$O)$_{6-x}$(OP(OH)$_3$)$_x$]$^{2+}$ (x = 1−4), and E$_6$ and E$_7$ denote the energies of clusters [Me-(H$_2$O)$_x$(OP(OH)$_3$)$_4$]$^{2+}$ (x = 0, 1).

The first stage shows the energy change of the stepwise substitution of H$_2$O by H$_3$PO$_4$ with the formation of [Me(H$_2$O)$_{6-x}$(OP(OH)$_3$)$_x$]$^{2+}$ (Me = Co, Mn, x = 1−4). The stepwise substitution of H$_2$O by H$_3$PO$_4$ is exothermic, but the reaction energies decrease in magnitude. However, no large difference in energy change between Mn^{2+} and Co^{2+} can be found in this stage. The second stage of energy changes correspond to the exclusion of water and the formation of [Me(H$_2$O)$_x$(OP-(OH)$_3$)$_4$]$^{2+}$ (Me = Co, Mn; x = 1, 0). Significant differences between Mn^{2+} and Co^{2+} were found; for example, [Me(H$_2$O)-(OP(OH)$_3$)$_4$]$^{2+}$ is formed endothermally by 34.8 and 54.7 kJ/

mol for Me = Co^{2+} and Mn^{2+}, respectively. Even large energy difference is found between the formation of [Co(OP(OH)$_3$)$_4$]$^{2+}$ and [Mn(OP(OH)$_3$)$_4$]$^{2+}$ (8.5 vs 69.5 kJ/mol). Therefore, a total energy difference (ca 81 kJ/mol) for the exclusion of two water molecules from the coordination sphere in [Me(H$_2$O)$_2$(OP-(OH)$_3$)$_4$]$^{2+}$ (Me = Co, Mn) may explain the difficulty of Mn^{2+} incorporation into the tetrahedral network.

Conclusions

The in situ XAS was employed in probing the incorporation of Mn^{2+} and Co^{2+} from the precursor gel to AlPO$_4$-5 microporous framework in hydrothermal synthesis process. XRD suggests that the long-range ordered crystal structure for both MnAPO-5 and CoAPO-5 appeared at 150 °C. However, Mn^{2+} and Co^{2+} are different in the incorporation behaviors for transformation from 6-fold to 4-fold structure, as unraveled by the in situ XAS investigation. The transition of Co^{2+} into the tetrahedral framework is via three stages and completed at 120−150 °C, while Mn^{2+} transfers to the pentacoordination at 200 °C and gets to the tetrahedral structure after crystallization for 30 min at 200 °C. The incorporation of Mn^{2+} is more difficult than that of Co^{2+}.

On the basis of the experimental results, the metal ions transformation process was proposed and DFT computations at the BLYP/GGA-DNP level were carried out on the intermediates [Me(H$_2$O)$_x$(OP(OH)$_3$)$_y$]$^{2+}$ (Me = Co or Mn; $x + y$ = 6, 5, or 4). The structure parameters for the optimized Co^{2+} and Mn^{2+} intermediates are in good agreement with the experimental data. On the other hand, the energy analysis suggests that the exchange reaction of H$_3$PO$_4$ with water in the hydrated metal ions is favorable on energy, while the exclusion of water from the intermediate results in an energy increase. Furthermore, the transformation energy of [Mn(OP(OH)$_3$)$_4$]$^{2+}$ is much higher than that of [Co(OP(OH)$_3$)$_4$]$^{2+}$, which rationally explains the diversities of Co^{2+} and Mn^{2+} in incorporation behaviors.

References and Notes

(1) Thomas, J. M. *Angew. Chem., Int. Ed.* **1999**, *38*, 3588.
(2) Hartmann, M.; Kevan, L. *Chem. Rev.* **1999**, *99*, 635.
(3) Weckhuysen, B. M.; Rao, R. R.; Martens, J. A.; Schoonheydt, R. A. *Eur. J. Inorg. Chem.* **1999**, 565.
(4) Thomas, J. M.; Raja, R.; Sankar, G.; Bell, R. G. *Acc. Chem. Res.* **2001**, *34*, 191.
(5) Cundy, C. S.; Cox, P. A. *Microporous Mesoporous Mater.* **2005**, *82*, 1.
(6) Arieli, D.; Delabie, A.; Groothaert, M.; Pierloot, K.; Goldfarb, D. *J. Phys. Chem. B* **2002**, *106*, 9086.
(7) Tan, J.; Liu, Z.; Bao, X.; Liu, X.; Han, X.; He, C.; Zhai, R. *Microporous Mesoporous Mater.* **2002**, *53*, 97.
(8) Christensen, A. N.; Norby, P.; Hanson, J. C. *Microporous Mesoporous Mater.* **1998**, *20*, 349.
(9) Christensen, A. N.; Norby, P.; Hanson, J. C. *Acta Chem. Scand.* **1997**, *51*, 249.
(10) Norby, P.; Hanson, J. C. *Catal. Today* **1998**, *39*, 301.
(11) Christensen, A. N.; Jensen, T. R.; Norby, P.; Hanson, J. C. *Chem. Mater.* **1998**, *10*, 1688.

(12) Linden, M.; Schunk, S. A.; Schuth, F. *Angew. Chem., Int. Ed.* **1998**, *37*, 821.

(13) Sankar, G.; Thomas, J. M.; Rey, F.; Greaves, G. N. *J. Chem. Soc., Chem. Commun.* **1995**, 2549.

(14) Rey, F.; Sankar, G.; Thomas, J. M.; Barrett, P. A.; Lewis, D. W.; Catlow, R. A. *Chem. Mater.* **1995**, *7*, 1435.

(15) Grandjean, D.; Beale, A. M.; Petukhov, A. V.; Weckhuysen, B. M. *J. Am. Chem. Soc.* **2005**, *127*, 14454.

(16) de Moor, P.-P. E. A.; Beelen, T. P. M.; van Santen, R. A. *J. Phy. Chem. B* **1999**, *103*, 1639.

(17) de Moor, P.-P. E. A.; Beelen, T. P. M.; van Santen, R. A.; Tsuji, K.; Davis, M. E. *Chem. Mater.* **1999**, *11*, 36.

(18) Walton, R. I.; Smith, R. I.; O'Hare, D. *Microporous Mesoporous Mater.* **2001**, *48*, 79.

(19) Polak, E.; Munn, J.; Barnes, P.; Tarling, S. E.; Ritter, C. *J. Appl. Crystallogr.* **1990**, *23*, 258.

(20) Weckhuysen, B. M.; Baetens, D.; Schoonheydt, R. A. *Angew. Chem., Int. Ed.* **2000**, *39*, 3419.

(21) Vistad, Ø. B.; Akporiaye, D. E.; Taulelle, F.; Lillerud, K. P. *Chem. Mater.* **2003**, *15*, 1639.

(22) Xiong, G.; Yu, Y.; Feng, Z. C.; Xin, Q.; Xiao, F. S.; Li, C. *Microporous Mesoporous Mater.* **2001**, *42*, 317.

(23) Calabro, D. C.; Valyocsik, E. W.; Ryan, F. X. *Microporous Mater.* **1996**, *7*, 243.

(24) Cheetham, A. K.; Mellot C. F. *Chem. Mater.* **1997**, *9*, 2269.

(25) Kornatowski, J.; Finger, G.; Jancke, K.; Richter-Mendau, J.; Schultze, D.; Joswig, W.; Baur, W. H. *J. Chem. Soc., Faraday Trans.* **1994**, *90*, 2141.

(26) Muncaster, G.; Davies, A. T.; Sankar, G.; Catlow, C. R. A.; Thomas, J. M.; Colston, S. L.; Barnes, P.; Walton, R. I.; O'Hare, D. *Phys. Chem. Chem. Phys.* **2000**, *2*, 3523.

(27) Mortlock, R. F.; Bell, A. T.; Radke, C. J. *J. Phys. Chem.* **1993**, *97*, 767.

(28) Mortlock, R. F.; Bell, A. T.; Radke, C. J. *J. Phys. Chem.* **1993**, *97*, 775.

(29) Robson, H., Ed. *Verified Syntheses of Zeolitic Materials*, 2nd ed.; Elsevier Science Publishers: Amsterdam, The Netherlands, 2001; p 96.

(30) Zhang, R. Z.; Qin, Z. F.; Dong, M.; Wang, G. F.; Wang, J. G. *Catal. Today* **2005**, *110*, 351.

(31) Liu, T.; Xue, C.; Xie, Y.; Hu, T.; Zhang, J.; Wu, Z. *Nucl. Tech.* **2004**, *27*, 885.

(32) Liu, T.; Xie, Y.; Hu, T. *Nucl. Tech.* **2004**, *27*, 401.

(33) Ressler, T.; Brock, S. L.; Wong, J.; Suib, S. L. *J. Phys. Chem. B* **1999**, *103*, 6407.

(34) Ressler, T.; Wienold, J.; Jentoft, R. E. *Solid State Ionics* **2001**, *141–142*, 243.

(35) Zabinsky, S. I.; Rehr, J. J.; Ankudinov, A.; Albers, R. C.; Eller, M. J. *Phys. Rev. B* **1995**, *52*, 2995.

(36) Delley, B. *J. Chem. Phys.* **1990**, *92*, 508.

(37) Delley, B. *J. Phys. Chem.* **1996**, *100*, 6107.

(38) Delley, B. *J. Chem. Phys.* **2000**, *113*, 7756.

(39) Delley, B. *Phys. Rev. B* **2002**, *66*, 155125.

(40) Becke, A. D. *J. Chem. Phys.* **1988**, *88*, 2547.

(41) Lee, C.; Yang, W.; Parr, R. G. *Phys. Rev. B* **1988**, *37*, 785.

(42) Norby, P.; Christensen, A. N.; Hanson, J. C. *Inorg. Chem.* **1999**, *38*, 1216.

(43) Henson, N. J.; Hay, P. J.; Redondo, A. *J. Phys. Chem. A* **2000**, *104*, 2423.

(44) Shannon, R. D. *Acta. Crystallogr.* **1976**, *A32*, 751.

(45) Flanigen, E. M.; Patton, R. L.; Wilson, S. T. In *Innovations in Zeolite Material Science*; Grobet, P. J., Mortier, W. J., Vansant, E. F., Schulz-Ekloff, G., Eds.; *Studies in Surface Science Catalysis 37*; Elsevier Science Publishers: Amsterdam, 1988; p 13.